Specific heat and ac susceptibility studies of the superconducting phase diagram of $PrOs_4Sb_{12}$

K. Grube,[1] S. Drobnik,[1,2] C. Pfleiderer,[2,*] H. v. Löhneysen,[1,2] E. D. Bauer,[3,†] and M. B. Maple[3]
[1]*Forschungszentrum Karlsruhe, Institut für Festkörperphysik, P.O. Box 3640, D-76021 Karlsruhe, Germany*
[2]*Physikalisches Institut, Universität Karlsruhe, D-76128 Karlsruhe, Germany*
[3]*Department of Physics and Institute for Pure and Applied Physical Sciences, University of California, San Diego, La Jolla, California 92093, USA*
(Received 29 August 2005; revised manuscript received 7 December 2005; published 8 March 2006)

We report on ac-susceptibility and heat-capacity measurements of the superconductor $PrOs_4Sb_{12}$ in magnetic fields. The resulting phase diagram reveals two distinguishable superconducting phases with transitions at the upper critical field B_{c2} and a slightly lower field B_{c2}^*. Between B_{c2}^* and $0.7\times B_{c2}^*$ the ac-susceptibility data shows a region with enhanced pinning properties characterized by an extended peak effect. The heat-capacity data reveal an extremely strongly coupled superconductivity with a considerable contribution of heavy quasiparticles. This unusual strong-coupling behavior originates in a sharp increase of the superfluid density at T_c. The decrease of the discontinuity of the specific heat at T_c and the corresponding pronounced increase of the Ginzburg-Landau-Maki parameter κ_2 indicate that the superconductivity is most probably not Pauli limited in a large temperature range.

DOI: 10.1103/PhysRevB.73.104503 PACS number(s): 74.70.Tx, 65.40.−b, 74.25.Ha, 71.27.+a

I. INTRODUCTION

The proximity of many Ce- and U-based heavy-fermion (HF) superconductors to magnetic order has led to the assumption that HF superconductivity is mediated by magnetic fluctuations. Extraordinary properties as line or point nodes of the superconducting gap and multiple superconducting phases support this assumption. The filled skutterudite compound $PrOs_4Sb_{12}$, the first Pr-based HF superconductor,[1] opens up the possibility of another, yet unknown, pairing mechanism. In contrast to Ce- and U-based HF systems the Pr^{3+} ions of $PrOs_4Sb_{12}$ have a nonmagnetic ground state and the heavy quasiparticles are not formed by the Kondo effect but presumably by excitations of the low-lying crystal electric field $4f^2$ levels, first described by White and Fulde[2] to explain the mass enhancement of elemental Pr.

An increasing amount of experimental data demonstrates the unconventional character of the superconductivity in $PrOs_4Sb_{12}$. Among others, these are the existence of at least two superconducting phases,[3,4] indication of point nodes in the superconductive gap,[5,6] the possible breaking of the time reversal symmetry in the superconducting state,[7,8] and an unconventional strong-coupling superconductivity as evidenced by Sb-NQR measurements.[9] Finally, the contribution of heavy quasiparticles to the superconducting condensate is confirmed by the large specific-heat jump at T_c, in contrast to the isostructural reference compounds $LaOs_4Sb_{12}$ and $PrRu_4Sb_{12}$, which are both conventional superconductors below 1 K.[10,11] In addition, the temperature dependence of the upper critical field B_{c2} shows a positive curvature near $T_c(B=0)$. Together with the rapid restoration of the normal thermal conductivity in small magnetic fields this might point to multiband superconductivity.[12,13] The occurrence of two distinct transitions has been discussed as evidence for superconductivity arising in two Josephson-coupled bands.[14]

Despite the increasing number of experimental and theoretical studies the essential properties of $PrOs_4Sb_{12}$ are still controversial and far from being understood. A double transition was observed not only in thermodynamic bulk measurements as specific heat[1,3,12,15,16] and thermal expansion,[17] but also in ac-susceptibility[4,12,18] and resistivity measurements[12] where in the latter two the very onset of superconductivity should disguise the observation of any other superconductive transitions. The strikingly similar magnetic field dependence of the transitions, has cast doubts on their intrinsic origin. Consequently, sample inhomogeneities due to impurities or stress have been proposed as possible explanations, but they could not explain the surprising consistency between an increasing number of measurements on samples of different origin.[1,3,4,12,14–20] Even more, at very small magnetic fields, deep in the superconducting state, recent high-precision magnetization studies revealed a pronounced enhancement of the lower critical field, possibly indicating a further superconducting phase, which, however, has to be verified by other thermodynamic bulk measurements.[4]

An intrinsic origin of multiple superconductive phases implies an additional symmetry breaking with a lower symmetry of the superconducting gap resulting from a multicomponent order parameter. In the only other known multiphase superconductors, UPt_3 and possibly $U_{1-x}Th_xBe_{13}$ ($0.01<x\leqslant 0.035$), as well as in the multiphase superfluid ^{3}He, the energy gap in the different superconducting phases shows different symmetries. Up to now, in $PrOs_4Sb_{12}$ only angle-resolved magnetothermal transport studies have yielded strong evidence for the existence of two distinct phases by distinguishing two dissimilar gap structures.[6] The phase diagram, however, deviates from all other published data.

While in $PrOs_4Sb_{12}$ all investigations have so far ruled out line nodes, evidence for point nodes is provided by penetration depth[5] and thermal conductivity measurements.[6] Tunneling spectroscopy,[21] Sb-NQR,[9] and μSR studies,[8,22] are compatible with an isotropic or nearly isotropic energy gap. Usually, the low-temperature behavior of the heat capacity

provides a simple test for nodes. In $PrOs_4Sb_{12}$, however, the first excited crystal electric field (CEF) level of the $4f^2$ Pr states is nearly degenerate with the ground state, with an energy difference accidentally close to the superconductive gap. Therefore, both states are altered considerably by magnetic fields, making a separation rather difficult. In addition, the formation of heavy quasiparticles in the normal state is masked by the large CEF contribution and nearly all estimates of large effective masses are so far deduced from superconducting properties as the discontinuity of the specific heat or the initial slope of the upper critical field $dB_{c2}/dT|_{B\to 0}$.[23]

The situation is further complicated by the extraordinary crystal structure of $PrOs_4Sb_{12}$. Its cubic unit cell with space group $T_h^5(Im\bar{3})$ comprises stiff Os_4Sb_{12} cages filled with loosely bounded Pr^{3+} ions. The Pr^{3+} ions exhibit anharmonic, rattling oscillations, most probably around off-center positions.[24] The resulting interaction between the Pr^{3+} ions and the CEF of the Os_4Sb_{12} cages might lead to a considerably broadening of the CEF excitation spectrum and even influence the superconductivity.

In order to clarify the phase diagram and to shed further light on the unusual normal and superconducting properties of $PrOs_4Sb_{12}$ we have performed heat-capacity and ac-susceptibility measurements on this compound.

II. SAMPLE PREPARATION AND QUALITY

All specific-heat and ac-susceptibility measurements were carried out on the same sample A unless stated otherwise. The cuboid-shaped single crystal of approximately $1\times1\times0.5$ mm^3 with a mass of 2.19 mg was grown from high-purity starting elements in a Sb flux. After the separation of the flux, excess Sb was removed from the sample surface by etching the crystals with diluted aqua regia.[25] The sample surface was studied by XPS microprobe analysis revealing a stoichiometric composition with small islands of Sb and Sb oxide (within the experimental resolution of 1 at. %), the latter having possibly been formed during the exposure of the sample to air. A single-crystal x-ray diffraction analysis of the sample was performed using a four-circle diffractometer and Mo $K\alpha$ radiation. The subsequent structure refinement with the aid of the SHELXS programm agrees with the values published by Ho *et al.*[26] and demonstrates a nearly complete occupation of the Pr site (see Table I).

In order to estimate the amount of diamagnetic Sb inclusions we chose five similar single crystals of the same batch with a total mass of $\approx$5 mg, being large enough to allow an x-ray powder diffraction study. The resulting diffraction pattern could be described by approximately 70% stoichiometric $PrOs_4Sb_{12}$ and 30% elemental antimony while Sb oxide was below the detection in the bulk. A small unidentified phase was witnessed by an additional peak. We measured the dc magnetization of the five powdered samples with a Quantum Design SQUID magnetometer at $B=5.5$ T. The temperature range was extended up to 400 K to reach the free-ion $4f^2$ state of the Pr^{3+} ions. The obtained inverse susceptibility $\chi_{dc}^{-1}(\chi_{dc}\equiv\mu_0 M/B)$ shows a linear temperature dependence above 30 K indicating standard Curie-Weiss behavior. A linear fit to the data in the range $30\ \mathrm{K}\leqslant T\leqslant 400\ \mathrm{K}$ gives a Curie-Weiss temperature of $\Theta_{CW}=-8.6\pm1$ K and an effective moment of $\mu_{eff}^{(exp)}=3.15\pm0.02\ \mu_B$ pointing to a significantly smaller Sb content of $12\pm6\%$. Thus, the magnetization studies seem to underestimate the excess Sb content although the origin of this discrepancy is not known. Returning to sample A, the dc magnetization measurement yields $\Theta_{CW}=-13.5\pm0.5$ K and $\mu_{eff}^{(exp)}=3.44\pm0.02\ \mu_B$. With the same discrepancy between x-ray and magnetization measurement, sample A may contain 12%–15% excess Sb.

TABLE I. Single crystal x-ray diffraction data and structure refinements of the $PrOs_4Sb_{12}$ samples A and B. The crystal structure belongs to the space group $Im\bar{3}$. U_{nn} is the thermal displacement factor. The occupancy (occ.) of the Os site was set to 1.

	Sample A	Sample B
a (Å)	9.301(4)	9.306(4)
Pr in 2a (0,0,0)		
$U_{11}=U_{22}=U_{33}$ (Å^2)	0.0386(10)	0.0384(7)
occ.	0.98(2)	0.98(2)
Os in 8c		
$U_{11}=U_{22}=U_{33}$ (Å^2)	0.0046(2)	0.0041(1)
Sb in 24g $(0,y,z)$		
y (Å)	0.15599(5)	0.15611(4)
z (Å)	0.34037(6)	0.34028(5)
U_{11} (Å^2)	0.0043(3)	0.0038(2)
U_{22} (Å^2)	0.0059(3)	0.0059(2)
U_{33} (Å^2)	0.0079(3)	0.0077(2)
occ.	0.99(2)	1.0(2)

All measured transition temperatures and critical fields of sample A show excellent agreement with measurements on other samples and with most of the published data. In contrast to this concurrent behavior, heat-capacity measurements demonstrate a strong sample dependence.

Specific-heat measurements performed on sample A (2.19 mg) and another very small sample B (0.58 mg) of the same batch are shown as C/T versus T in Fig. 1. At $T>1.0$ K, the data agree with each other and with other reported measurements in their overall T dependence, but differ strongly in their absolute values (see inset of Fig. 1). The data of sample A are 14%, 16%, and $33\pm5\%$ smaller than the data reported by Aoki *et al.*,[15] Measson *et al.*,[12] and the data points of sample B, respectively. The discontinuity at T_c tends to show a better resolved double transition in samples with higher C/T values. If data are scaled by a T independent factor r (see caption to Fig. 1), they fall on top of each other between 10 K and 1 K. Below 1.0 K, however, the upturn in the heat capacity varies from sample to sample but seems to be smaller in samples with enhanced specific heat.

This suggests that the differences might be due to varying amounts of Sb inclusions. While this trend is consistent with varying Sb content, the upturn in C cannot be explained by Sb exclusively, because the contribution of the nuclear hyperfine contribution to C of pure Sb is two orders in magni-

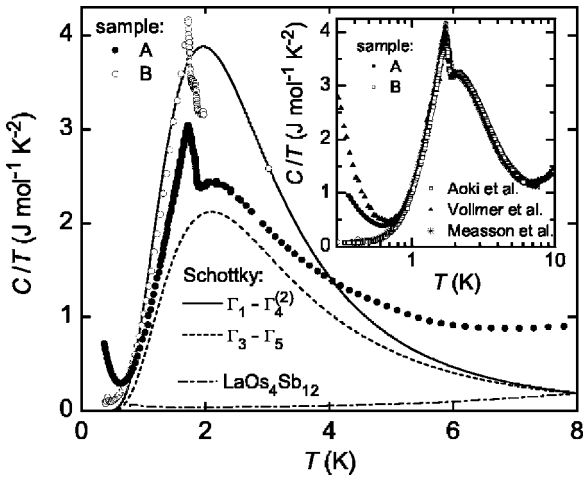

FIG. 1. The measured specific heat divided by temperature, C/T, at zero-magnetic field of two different samples of the same batch. For comparison the calculated Schottky contributions are shown for the crystalline electric field transitions: doublet-triplet (Γ_3-Γ_5) and singlet-triplet (Γ_1-$\Gamma_4^{(2)}$ equivalent to Γ_1-Γ_5 in a fully symmetric cubic system), together with C/T of $LaOs_4Sb_{12}$ (Ref. 25). The inset shows the following C/T measurements multiplied by a factor r to fit the data of sample B: sample A ($r=1.33$) and measurements from Vollmer *et al.* (Ref. 3) ($r=1.29$), Measson *et al.* (Ref. 12) ($r=1.1$), and Aoki *et al.* (Ref. 15) ($r=1.16$).

tude smaller. On the other hand, any stress in the crystals or any off-center position of the Pr^{3+} ion that breaks the cubic site symmetry could give rise to an increased hyperfine contribution of the Pr^{3+} ions.

The mass of sample B is too small to allow a reasonable determination of its Sb content with a dc magnetization measurement. An x-ray diffraction study and subsequent structure refinement, however, could not reveal any striking differences to sample A at room temperature (see Table I).

As the magnetic moment of sample B falls below the resolution limit of our ac susceptometer we performed all measurements on the same sample A. In the following, all quantities extracted from specific-heat measurements of sample A will be given, as measured, followed by the 33% higher values in parentheses to show the probable range of these quantities (assuming the "worst case" of maximal excess Sb content).

III. EXPERIMENTAL METHODS

The ac susceptibility χ was measured with a miniature susceptometer, comprised of a primary coil surrounding a balanced pair of secondary coils. Typical excitation fields were smaller than $B_{ac} \leqslant 0.05$ mT at a frequency of 234 Hz. The small signal of the empty susceptometer was essentially featureless in the entire measured temperature and magnetic field range of 20 mK $\leqslant T \leqslant 4$ K and $B \leqslant 2$ T, respectively.

The specific heat C was measured by means of a conventional heat-pulse technique using a Physical Property Measurement System (PPMS) from Quantum Design. Data were taken as a function of temperature as low as 0.35 K and magnetic field as high as 14 T. The magnetic-field dependent addenda were measured separately at the identical fields and subtracted from the measurements. The relative resolution of the measurements was better than 0.5% with an absolute accuracy of 1%. Our data agree with those taken with a homebuilt system in a dilution cryostat in previous studies in the range of overlap.[3]

IV. SPECIFIC HEAT

In Fig. 1 the low-temperature specific heat divided by temperature C/T is plotted as a function of T at zero magnetic field. The comparison with the heat capacity of the reference compound $LaOs_4Sb_{12}$ shows that in the temperature range displayed, C/T of $PrOs_4Sb_{12}$ is mainly produced by the $4f^2$ states of the Pr^{+3}.

The C/T data are dominated by a broad peak at $T \approx 2$ K. Recent neutron-scattering studies have determined the CEF splitting of the ninefold degenerate $4f^2$ state of the Pr^{3+} ions. We thus identify this peak as a Schottky anomaly caused by a singlet-triplet transition between the lowest CEF levels, roughly, $\Gamma_1(0)$-$\Gamma_4^{(2)}(7.8\ \mathrm{K})$-$\Gamma_4^{(1)}(135\ \mathrm{K})$-$\Gamma_{23}(205\ \mathrm{K})$.[27–29] In a quantitative analysis, our specific-heat measurements and, to our knowledge, all published heat-capacity data appear to contradict this level scheme. Although the position of the anomaly agrees with the energy difference to the first excited level, the smaller height of the measured peak points to a transition with a clearly reduced entropy. The C/T data of sample A are more than 60% below the expected values and C/T of sample B more than 20±5% (see Fig. 1). The specific-heat data in zero magnetic field seem to favor the originally proposed CEF level splitting with a doublet as ground state and a triplet as a first excited level, approximately $\Gamma_3(0)$-$\Gamma_5(8.2\ \mathrm{K})$-$\Gamma_4(133.5\ \mathrm{K})$-$\Gamma_1(320\ \mathrm{K})$ (Refs. 1, 3, and 10) (see the dashed line in Fig. 1).

On the other hand, specific-heat measurements in applied magnetic fields clearly support a singlet ground state because states with higher degrees of freedom should split in magnetic fields. Even nonmagnetic, non-Kramers doublets, as Γ_3, exhibit a higher-order magnetic-field dependence due to the Van Vleck susceptibility as illustrated by the calculated CEF level schemes of $PrOs_4Sb_{12}$.[3,19] The splitting leads inevitably to a large Schottky anomaly, moving to higher temperatures with growing field. Neither our measurements nor published studies could reveal such anomalies.[3,15]

Again the discrepancy between measured and theoretically expected CEF contribution to C is too large to be explained by antimony inclusions exclusively. Apart from any impurity phases, lattice distortions due to stress, off-center positions of the Pr^{3+} ions, the rattling modes, the hybridization of the $4f^2$ states with the conduction band, and, finally, any interaction between the $4f^2$ moments could alter the CEF splitting, broaden the Schottky anomaly and shift entropy to higher temperatures.

The transition to superconductivity is clearly visible as a large, broadened mean-field discontinuity superimposed on the Schottky anomaly. In small magnetic fields the discontinuity is rapidly suppressed and shifted to lower temperatures until it vanishes for $B > 2$ T (see Fig. 2). With a slightly weaker field dependence, the Schottky peak also moves to

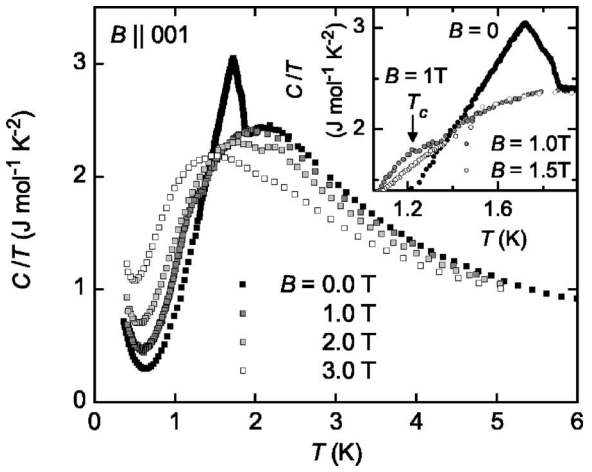

FIG. 2. The specific-heat coefficient C/T measured at several constant magnetic fields as a function of T. The Schottky anomaly at $T \approx 2$ K shows a smaller field dependence than the discontinuity at the superconducting transition temperature. In the inset the zero-field data are depicted together with measurements at $B = 1.0$ T and 1.5 T which could serve approximately as a normal conducting background for the zero-field specific heat.

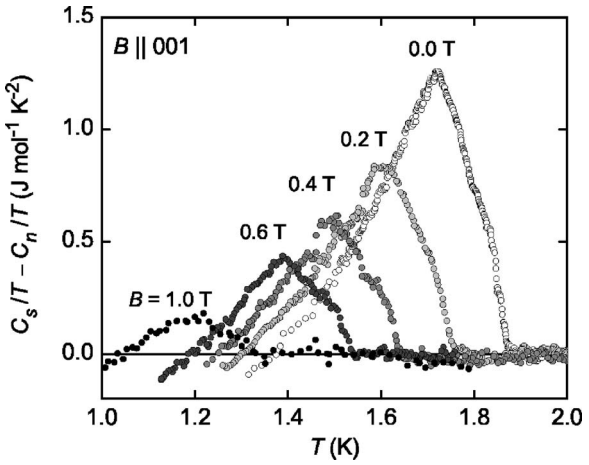

FIG. 3. Typical differences between the superconductive and normal-state specific heat divided by temperature in constant magnetic fields. The normal-state contribution has been subtracted as described in the text. The discontinuity exhibits the double transition as two rounded jumps at T_c and T_c^* (with $T_c > T_c^*$). With increasing magnetic field the transitions are shifted to lower T with rapidly diminishing discontinuities.

lower temperatures, indicating the magnetic-field induced splitting of the first excited CEF triplet.

In order to analyze the superconductive part of C/T, C_s/T, usually the specific heat in the normal state and the magnetic-field dependent CEF contributions have to be subtracted. For $PrOs_4Sb_{12}$, two such analyses have so far been published: Vollmer *et al.*[3] used a CEF level scheme with a doublet Γ_3 ground state and Frederick *et al.*[11] additionally a modified level scheme with a singlet Γ_1 ground state. Depending on the CEF ground state used, the data differ from one another and exhibit different normal-state contributions. These analyses are hampered by the sample dependence of C and its deviation from the expected CEF behavior. Another possibility for determining C_s/T relies on the fact that the position of the Schottky anomaly varies comparatively slowly with increasing field, so that at moderate fields, where the superconductivity is not completely suppressed, the normal-state heat capacity could serve as background at $T > T_c(B > 0)$ (see Fig. 2). The inset of Fig. 2 demonstrates that at least down to $T \approx 1.5$ K, the C/T measurement at $B = 1.0$ T represents, to a good approximation, the normal-state background C_n/T. At lower T and/or for $B > 1.0$ T, however, the change of the Schottky anomaly is too large to warrant a reliable construction of C_n/T. Here, the normal-state C/T data below T_c were obtained by assuming a scaling of the Schottky anomaly with T/B as expected. In addition for the lowest temperatures between 0.5 K and 0.7 K the contribution of the hyperfine coupling has to be substracted which was modelled with T^{-2}. The resulting differences $C_s/T - C_n/T$ are displayed in Fig. 3. The curves shown in Fig. 3 exhibit a double transition as two rounded jumps at T_c and T_c^* ($T_c^* < T_c$) followed by a very sharp decrease of $C_s/T - C_n/T$ towards lower T. With increasing field both transitions are pushed to lower T while the discontinuities are reduced and broadened.

In Fig. 4 the zero-field $C_s/T - C_n/T$ data are plotted down to 0.5 K. As mentioned before, the uncertainty in constructing C_n/T increases with decreasing temperature. The error bars in Fig. 4 represent two possible limits of the background construction. The lower limit is given by taking the normal-state part of C/T at $B > 1$ T without any scaling. Due to the field-dependent shift of the Schottky anomaly to lower temperatures this leads to an *overestimation* of the background. For the upper limit the normal-state part of C/T are shifted to

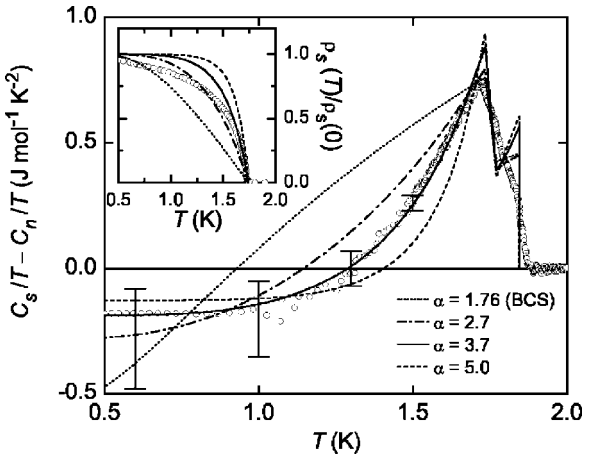

FIG. 4. The difference between superconductive and normal-state specific heat divided by temperature. The construction of C_n/T and the meaning of the error bars is described in the text. For comparison model calculations are shown that display the weak- and strong-coupling behavior of a conventional, isotropic superconductor with different gap ratios $\alpha = \Delta(0)/k_B T_c$ (for details see text). The data are best described by extremely strong-coupling superconductivity. The inset shows the normalized superfluid density derived from penetration depth measurements from Chia *et al.* (Ref. 5) (circles) together with the corresponding model calculations. The pronounced increase of $\rho_s(T)/\rho_s(0)$ below $T < T_c^* \approx 1.75$ K is apparently reflected in the sharp decrease of C_s/T towards lower T.

the zero-field position of the Schottky anomaly. In this case the background is *underestimated* because the broadening of the Schottky anomaly with temperature is not taken into account. Despite the uncertainties at higher fields and lower temperatures, the integration of the zero-field $C_s/T-C_n/T$ data yields the expected entropy balance, $S_s(T_c)=S_n(T_c)$, if the data are linearly extrapolated from the lowest measured temperature to $T\rightarrow 0$. Hence the entropy consideration provides an independent cross-check of our analysis.

The rapid decrease of $C_s/T-C_n/T$ at $T<T_c^*$ shown in Fig. 4 is a characteristic feature of strong-coupling superconductivity. In the BCS weak-coupling limit, $C_s/T-C_n/T$ becomes zero at approximately $0.5\cdot T_c$ while the depicted data exhibit the zero crossing at $0.7\pm 0.05\cdot T_c$. In the former attempts to extract C_s/T, published by Vollmer *et al.*[3] and Frederick *et al.*,[11] C_s/T crosses C_n/T between $0.6\cdot T_c$ and $0.7\cdot T_c$.

In order to demonstrate the uniqueness of this behavior, we fit our data with the so-called α-model. Padamsee *et al.*[30] who developed the model, assumed that superconductive properties which are mainly influenced by the size of the gap and the quasiparticle-state occupancy could be approximated by simply using the temperature dependence of the weak-coupling BCS gap. The size of the gap is a freely adjustable parameter $\alpha=\Delta(0)/k_BT_c$, where $\Delta(0)$ is the (Fermi-surface averaged) gap at $T=0$. In our case the only other free parameter is the normal-state electronic specific heat, represented by the Sommerfeld coefficient γ, because the not fully understood CEF contributions prevent us from determining γ directly. The specific heat is calculated by differentiating the entropy

$$S/(\gamma T_c) = -6\alpha/\pi^2 \int_0^\infty [f\ln(f) + (1-f)\ln(1-f)]dE, \quad (1)$$

according to $C_s/T-C_n/T=\gamma(d(S/(\gamma T_c))/dt-1)$. The quasiparticle-state occupancy is given by $f=[\exp(\alpha/t\cdot\sqrt{E^2+\Delta(t)^2})+1]^{-1}$ and $t=T/T_c$. For the temperature dependence of the gap $\delta(T)=\Delta(T)/\Delta(0)$, we used the values tabulated by Muehlschlegel.[31] Due to the difference $C_s/T-C_n/T$, the gap ratio α determines the zero point of the calculated curve, while γ controls the height of the discontinuity. We fitted the data with a single transition and two independent transitions. The latter reflects the behavior of either an inhomogeneous sample comprised of two fractions with different T_c's or a two-band superconductor with two completely independent bands and different T_c's. A scenario in which the two phases depend on each other, i.e., a second symmetry breaking due to a multicomponent order parameter, are beyond the capabilities of this simple model. As both discontinuities are approximately of the same size and behave similarly in magnetic fields, we choose equal gap ratios and Sommerfeld coefficients. Both approaches, with the single and the double transitions, lead to the same results. Figure 4 shows the fits in which the two transitions are modelled. The calculations in the weak-coupling limit deviate considerably from the observed behavior. The pronounced shape of the discontinuity and the zero-crossing point at high temperatures are best described by an extremely strong-coupling scenario with a gap ratio of $\alpha=3.7\pm 0.2$ (BCS: $\alpha=1.76$) (Ref. 32) and a total Sommerfeld coefficient of $\gamma=0.2\pm 0.05(0.27\pm 0.07)$ J K^{-2} mol^{-1}. The normalized specific-heat jump amounts to $\Delta C/(\gamma T_c)\approx 5\pm 1(6.7\pm 1.3)$ (BCS: $\Delta C/(\gamma T_c)=1.43$).[32] Usually, HF superconductors are not in the extreme strong-coupling regime. The only exception which is comparable to $PrOs_4Sb_{12}$ is $CeCoIn_5$ with a specific heat jump of $\Delta C/(\gamma T_c)=4.5$ and a gap ratio of $\alpha=4.43$, that even exceeds our value.[33,34] The lower value of γ as compared to previous analysis is supported by measurements of the upper critical field (see the end of this section). The obtained values of the α-model analysis of our measurements and literature data are listed in Table II.

TABLE II. Summary of the α-model analysis of the superconductive part of our zero-field specific heat measurement and published C_s data of $PrOs_4Sb_{12}$. Γ_1 and Γ_3 correspond to a background substraction assuming a singlet or doublet CEF state, respectively. Due to the uncertainity of the extraction of C_s at low temperatures, we fitted the α-model only to data points above 1.2 K. In this fit, the linear specific heat coefficient γ is determined by the height of the discontinuity (any varying excess Sb content is not taken into account).

Specific heat data	$\alpha=\Delta(0)/k_BT_c$	γ (J mol^{-1} K^{-2})
This work (see Fig. 4)	3.7±0.2	0.20±0.05
Vollmer *et al.*[a]	2.6±0.2(Γ_3)	0.35±0.05
Frederick *et al.*[b]	3.1±0.2(Γ_1)	0.26±0.05
Frederick *et al.*[b]	3.6±0.2(Γ_3)	0.21±0.05

[a]Reference 3.
[b]Reference 11.

The specific heat is closely related to the temperature dependence of the superfluid density $\rho_s(T)$. Therefore, to verify this extraordinary behavior of C, we used again the simple assumption of the α-model and calculated $\rho_s(T)$ according to Bouquet *et al.*[32,35]

$$\rho = 1 - 2\alpha \int_0^\infty f(1-f)dE. \quad (2)$$

The inset of Fig. 4 shows the penetration depth data reported by Chia *et al.*,[5] $\rho_s(T)/\rho_s(0)=\lambda(0)^2/\lambda(T)^2$ and the calculations of the α-model assuming the same gap ratios as in

TABLE III. Summary of the published superconductive gap ratios and gap anisotropy of $PrOs_4Sb_{12}$.

Experiment	$\alpha=\Delta(0)/k_BT_c$	Gap function
Tunneling spectroscopy[a]	1.7	Nearly isotropic
μSR[b]	2.1	Nearly isotropic
$\lambda(T)$[c]	2.6	Point nodes
Sb-NQR[d]	2.7	Isotropic

[a]Reference 21.
[b]Reference 22.
[c]Reference 5.
[d]Reference 9.

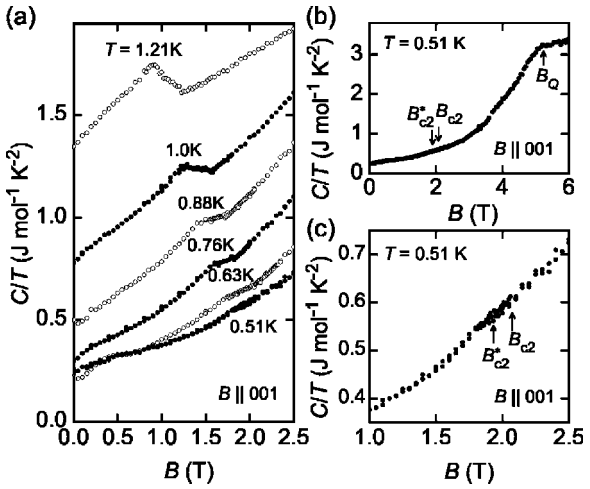

FIG. 5. (a) The specific heat divided by T as a function of the magnetic field B. (b) C/T at $T=0.51$ K in fields up to $B\leqslant 6$ T. Note the strongly field-dependent normal-state background up to the onset of the field induced phase at $B_Q\approx 5$ T. (c) Enlarged section of (b) with the discontinuities at B_{c2}^* and B_{c2} that have almost vanished.

Fig. 4. The pronounced increase of $\rho_s(T)$ just below the onset of superconductivity appears to be best described by the same large gap ratio of 3.7. With decreasing temperature, however, the data deviate more and more from the fit and approach finally the reduced values of the weak-coupling scenario. A simple explanation of this behavior are nodes in the gap function which give rise to additionally unpaired quasiparticles. Indeed, below $T<0.6$ K, Chia *et al.*[5] demonstrated that the best fit is given by a gap function with two point nodes and a still strongly enhanced gap ratio of 2.6. We want to stress that the α-model we used was developed for conventional, isotropic superconductors. Consequently, it can only confirm the precipitous condensation of quasiparticles, reflected in an extremely peaked specific heat, and does not cover the influence of nodes, multiple bands which interact with each other, or temperature dependent quasiparticle masses or coupling strengths.

Apart from penetration depth measurements, Sb-NQR, and μSR investigations also point to strong-coupling superconductivity (see Table III). Tunneling spectroscopy measurements, however, which probe the gap size directly, reveal a gap of 270 μeV at $T=0.19$ K and a ratio of 1.7, close to the BCS prediction. All these measurements indicate a nearly isotropic gap with no line nodes.

Maki *et al.*[36] and Parker *et al.*[37] have performed model calculations of C_s which are based on gap functions with point nodes and two phases with a two- and fourfold rotation symmetry. A comparison shows that they are not consistent with our measurements because they do not reproduce the strong-coupling behavior.

Figure 5(a) shows C/T as a function of B for various temperatures. Between 1.24 K and 0.76 K, C/T increases roughly linear with B, with a sublinear increase for lower T. This increase resides on a large B and T dependent C/T "background" up to the onset of the so-called field-induced ordered phase[38] [see Fig. 5(b)] due to the Schottky anomaly. Therefore, although models for the field dependence of C/T for nodal[39,40] and multiband[41] superconductors are at hand, we refrain from further discussion.

With decreasing T, the specific-heat jumps $\Delta C(B_{c2}^*)/T$ and $\Delta C(B_{c2})/T$ are diminished and shifted to higher fields. At the lowest temperature measured, $T=0.51$ K, the discontinuities have nearly disappeared [see Fig. 5(c)]. From the data measured at $T=0.51$ K, we can estimate an upper limit of the Sommerfeld coefficient by $\gamma<(C(B_{c2})/T-C(0)/T)=0.35(0.47)$ J mol^{-2} K^{-2}. This seems to confirm a moderate enhanced effective mass while a strong increase of γ at $T\rightarrow 0$, comparable to that of $CeCoIn_5$, seems to contradict these experimental findings.

V. AC SUSCEPTIBILITY

Figure 6 shows raw data of typical differential ac-susceptibility traces of the real (χ') and imaginary part (χ'') for $T=0.1$ K and 2 K as a function of superimposed dc magnetic fields. A dominant feature around 1 T is a change of the curvature of χ' and a broad minimum in χ'', which are independent of temperature up to 4 K. This feature is neither present for the empty susceptometer nor in any temperature dependent measurement of the sample at constant magnetic field. However, its mere size as compared with contributions of superconductivity of the sample, shown in panels (b) and (c), suggest that it originates from an electronic interference, e.g., resonance, of unexplained nature. For the analysis of our data, we have taken the field sweep at $T=2.0$ K as background, comprising contributions of the empty susceptometer with the sample in its normal state.[42]

The corrected differential susceptibilities in the superconducting state after subtraction of the background, $\Delta\chi=\chi(T)-\chi(T=2\text{ K})$, are shown in Figs. 6(b) and 6(c). The real part reflects the shielding behavior of the sample while the imaginary part reveals its irreversible properties, i.e., the energy dissipation $W=MdB=\pi\chi''B_{\text{ac}}^2$ which is just the area enclosed by the small hysteresis loop $M(B_{\text{dc}}+B_{\text{ac}}\cos(\omega t))$. The irreversible properties originate from the flux pinning of the vortice lattice. In reversible type-II superconductors with no pinning centers, $\chi''\approx 0$, and χ' represents the equilibrium differential susceptibility $\chi'=dM/dH$.[43] In this case, χ' is positive between B_{c1} and B_{c2}, the so-called differential paramagnetic effect, and the discontinuity at B_{c2} can be related to the jump of the specific heat.[44]

All measurements shown in Fig. 6 demonstrate large $\Delta\chi''$ values and a negative step of $\Delta\chi'$ near B_{c2} pointing to irreversible magnetic behavior. We focus therefore on the signature of phase transitions and the irreversible properties of the sample. The onset of superconductivity at B_{c2} is visible as the onset of a signal in $\Delta\chi'$ and $\Delta\chi''$. While $\Delta\chi'$ becomes negative, indicating shielding currents, $\Delta\chi''$ shows a broad ridge with a pronounced peak near the second transition B_{c2}^*. B_{c2}^* appears as inflection point in the real part. In $\Delta\chi''$ only B_{c2}^* is clearly observable while B_{c2} marks the sluggish onset of irreversible behavior. Besides the signature of the transitions we observe a well developed minimum in $\Delta\chi'$ and a peak in $\Delta\chi''$ indicating enhanced pinning properties. This so-called peak effect is a well-known feature of many con-

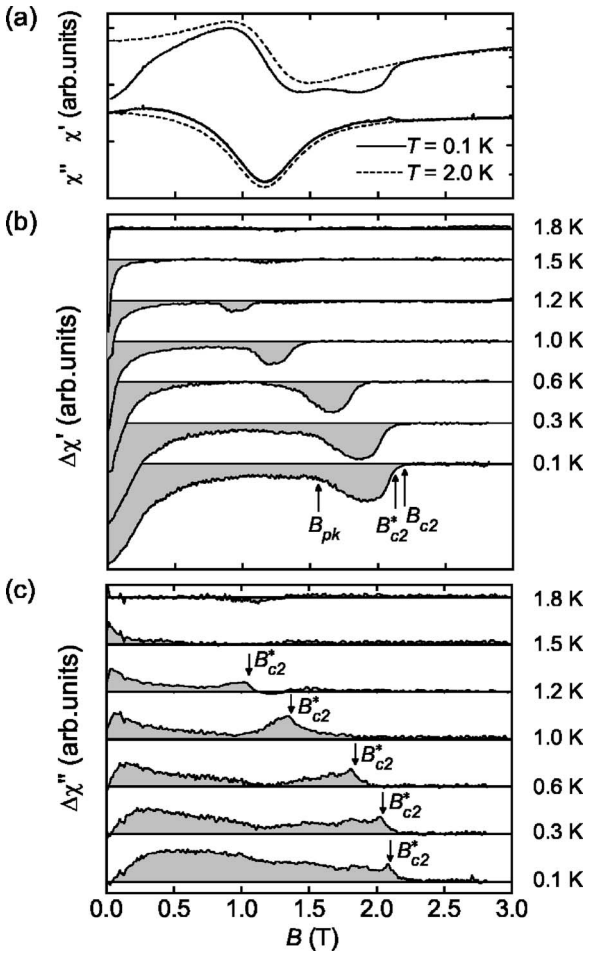

FIG. 6. ac susceptibility traces as function of magnetic field B in $PrOs_4Sb_{12}$. The curves are shifted with respect to another to facilitate their readability. (a) Typical raw data in the normal and superconducting state. Note the anomaly around 1 T, reminiscent of a resonance of unknown origin present only in the susceptometer with the sample added. (b) Typical contributions to the superconductivity of the real part of the corrected susceptibility $\Delta\chi=\chi(T)-\chi(T=2\ \mathrm{K})$. The two superconducting phase transitions are visible as slope changes at B_{c2} and B_{c2}^*. The minimum between B_{c2}^* and B_{pk} marks the peak effect. (c) Contributions of the imaginary part $\Delta\chi''$. Only the second transition B_{c2}^* can be identified approximately by the pronounced peak.

ventional and HF superconductors, e.g., UPd_2Al_3.[45] In $PrOs_4Sb_{12}$, it was also observed in dc magnetization and resistivity measurements.[19,46]

Towards smaller fields, $\Delta\chi'$ decreases abruptly and $\Delta\chi''$ vanishes. The restoration of reversible behavior together with the strongly enhanced shielding currents characterize the onset of the Meissner-Ochsenfeld state. Within the limited resolution of our measurement a rough estimate gives a maximum of the lower critical field of $B_{c1}<0.01$ T in agreement with published data.[4,46]

In Fig. 7, typical temperature dependent ac-susceptibility measurements are displayed together with the specific-heat data at constant magnetic fields of $B=0$ and 1.0 T. The double transition seen in the ac susceptibility corresponds to the two steps in the specific heat. In magnetic fields, $\Delta\chi'$

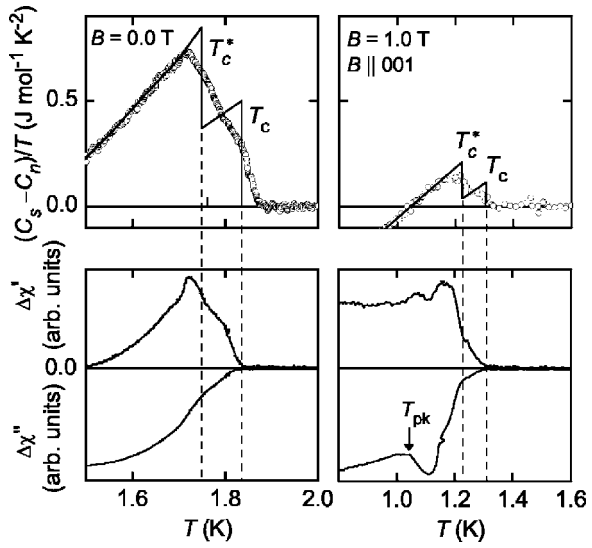

FIG. 7. Comparison between the corrected specific heat $C(T)$ and ac susceptibility $\chi(T)$ at constant magnetic fields $B=0$ and 1.0 T. The two superconducting transitions T_c and T_c^* can be identified as two broad steps in C. The susceptibility reflects the transitions as slope changes in $\Delta\chi'$ and maxima in $\Delta\chi''$. At $B=1.0$ T the peak effect produces a minimum between T_{pk} and T_c^*. Between onset of C and χ a small offset may be due to a slight difference in temperature calibration.

again shows a minimum demonstrating the enhanced shielding of the peak effect which, of course, is absent in C.

VI. PHASE DIAGRAM

In Fig. 8 the specific-heat and ac-susceptibility data are summarized in a (B,T) phase diagram. With decreasing temperature, the first observation of superconductivity appears at $T_c=1.86$ K with an upper critical field, $B_{c2}(T)$, which increases up to $B_{c2}(0)=2.3$ T. The second transition $B_{c2}^*(T)$ starts at $T_c^*=1.75$ K, tracks $B_{c2}(T)$, and reaches finally $B_{c2}^*(0)=2.1$ T. Both transitions show a similar magnetic-field dependence and can be scaled to one another with approximately the same scaling factors for the B and T axis: $B_{c2}^*(0)/B_{c2}(0)\approx T_c^*(0)/T_c(0)$. The signatures of B_{c2} and B_{c2}^* found in ac-susceptibility and specific-heat measurements agree perfectly with each other and are consistent with most of the available data, e.g., specific-heat,[1,3,12,15,16] magnetization,[19] thermal expansion,[17] ac-susceptibility,[4,12,18] and resistivity studies.[12,23,26]

The observation of two subsequent, superconducting transitions in ac-susceptibility measurements usually implies sample inhomogeneities. The approximately similar size of the specific-heat jumps indicates, that in this case two distinct, macroscopic parts of the sample have to become superconducting. A comparison of the available measurements which resolve the double transition reveals surprisingly different shapes of the discontinuities. While differences in ac-susceptibility and resistivity measurements are easily understood in terms of surface and contact effects, the small but significant differences in the size of the specific-heat

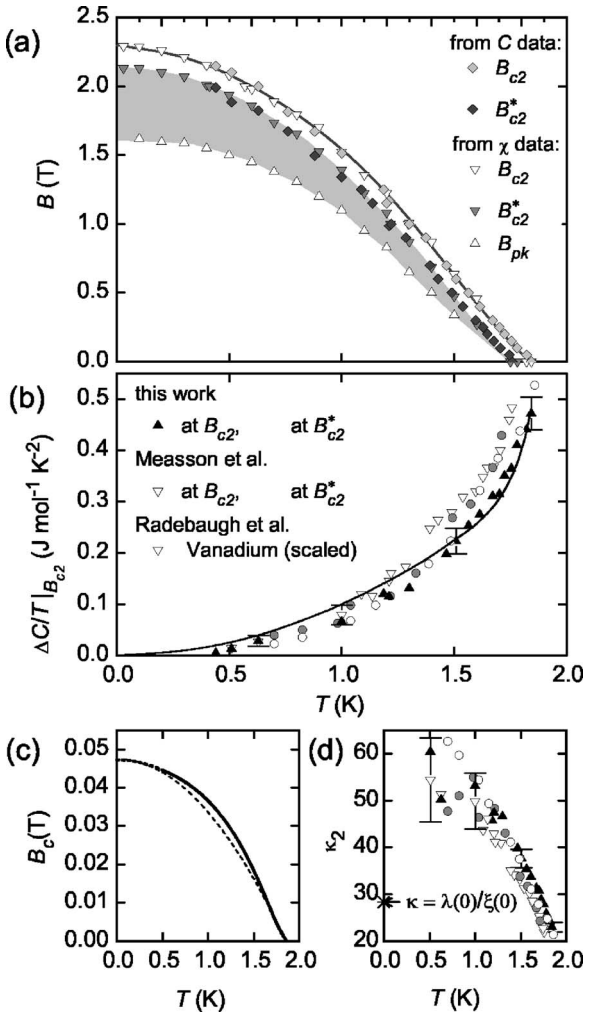

FIG. 8. Summary of specific-heat and ac-susceptibility data. (a) Phase diagram derived from the ac-susceptibility and specific-heat data. See Figs. 6 and 7 for the definition of B_{c2}, B^*_{c2}, B_{pk}, and T_c, T^*_c. Hatched area indicates the region of enhanced pinning properties. (b) The specific-heat jumps ΔC as a function of the transition temperatures T^*_c and T_c together with the data from Measson *et al.* (Ref. 12). The comparison with ΔC of vanadium from Radebaugh *et al.* (Ref. 47) indicates a rather conventional decrease of ΔC. (c) The thermodynamic critical field calculated from the specific-heat data shown in Fig. 4. The dashed line represents the extrapolation to zero temperature. The thin dashed line is the corresponding two-fluid model. (d) The Ginzburg-Landau parameter κ_2 calculated from the specific-heat jumps is displayed in (b). Further details are described in the text.

jumps[1,3,4,48,49] point again to two distinct sample fractions with different T_c and varying mass. Otherwise, if the differences have an intrinsic origin, they should result in different phase diagrams because ΔC is closely related to the magnetic field derivatives of the critical fields via the Ehrenfest relations.

Apart from the phase boundaries, Fig. 8 shows the temperature and field dependence of the peak effect, characterized by the enhanced shielding above B_{pk}. The peak effect tracks $B_{c2}(T)$ over the entire temperature range and reaches finally $B_{\mathrm{pk}}(0)=1.6$ T. Its temperature dependence proves clearly that it cannot be caused by matching effects where its occurrence is fixed to distinct, temperature-independent magnetic fields.[50] Likewise, the pinning on a second phase with slightly lower T_c is rather unlikely. Even if the double transition might signify such a phase the maximum of the peak effect should then be centered around B^*_{c2}. The measurements, however, show unambiguously that the peak effect disappears at B^*_{c2}. Due to the similar behavior of many conventional superconductors, the most probable explanation are weak pinning effects at impurities (see Table III).

It should be noted that the enhanced pinning properties might play an important role in stabilizing superconducting phases which have a smaller symmetry than the crystal structure. Magnetothermal transport studies point to a low-field superconducting phase with two point nodes and a reduced twofold rotation symmetry.[6] The resulting phase boundary of this low-temperature phase, however, deviates strongly from all other published measurements with a zero-temperature critical field of just $B\approx 0.8$ T. If the phase is aligned to the crystal lattice by pinning effects, the phase transition is controlled by the irreversible properties of the crystal and may differ from the thermodynamic, reversible phase boundaries found in other experiments.

Conventional and HF superconductors which are Pauli limited exhibit a characteristic increase of the discontinuity of the reversible susceptibility $\chi_{\mathrm{rev}}=\mu_0\,\partial M/\partial B|_{B_{c2}}$ with decreasing temperature. Due to the reduction of the upper critical field by the Pauli-paramagnetic lowering of the normal-state free energy, χ_{rev} becomes larger with increasing field and B_{c2} in comparison to B_{c1} smaller. Expressed in the Ginzburg-Landau-Maki parameter κ_2, one expects therefore a saturation or even decrease of κ_2 at high magnetic fields.[45,51] As mentioned before, we could not employ our ac-susceptibility measurements to determine χ_{rev}. Therefore, we turn to the discontinuity of the specific heat and estimated χ_{rev} via the Ehrenfest relation $\Delta\chi_{\mathrm{rev}}=1/\mu_0\cdot\,\Delta C/T|_{B_{c2}}(dB_{c2}/dT)^2$. Then κ_2 is given by

$$\kappa_2=\sqrt{(dB_{c2}/dT)^2/(2\beta\mu_0\Delta C/T)-1}, \tag{3}$$

where β is a number of order unity that depends on the vortex-lattice configuration.[52] The specific-heat jumps were obtained by an entropy-conserving method, as shown in Fig. 7, from our data and the measurements reported by Measson *et al.*[12] β was assumed to be 1.16 according to a triangular vortex lattice.[32] The obtained $\Delta C/T|_{B_{c2}}$ data are displayed in Fig. 8(b). The discontinuities are characterized by a pronounced decline when a magnetic field is applied. A comparison with the $\Delta C/T|_{B_{c2}}$ data of vanadium demonstrates that the data points follow the behavior of a conventional, weak-coupling superconductor surprisingly well. Figure 8(c) shows the deduced Ginzburg-Landau-Maki parameter κ_2 for B_{c2} and B^*_{c2} as a function of T. With decreasing T, κ_2 exhibits a strong enhancement. The missing saturation or decrease argues against Pauli-limited superconductivity, at least down to the lowest measured temperature $T=0.52$ K. The κ_2 values obtained are in rough agreement with the directly determined $\kappa=\lambda(0)/\xi_0\sim 3440$ Å/113 Å=30.4.[22,46]

Finally, we made a rough estimate of the thermodynamic critical field B_c and the condensation energy of E_c by integration of $C_s/T-C_n/T$ shown in Fig. 4 from 0.5 K to T_c. The low-temperature part was extrapolated by a parabola according to the thermodynamic condition $dB_c(0)/dT=0$. The condensation energy amounts to $E_c=210\pm20(280\pm30)$ mJ/mol. The resulting B_c exhibits again extreme strong-coupling behavior as the value of the corresponding two-fluid model $B_c^{\mathrm{fl}}=B_c(0)(1-(T/T_c)^2)$ is in the entire temperature range below B_c. The values are somewhat smaller than the rough estimate by $B_c=\sqrt{B_{c1}B_{c2}}$ with the values from Ho *et al.*[46] and Cichorek *et al.*[4] Similar to the upper critical fields B_{c2} and B_{c2}^*, B_c exhibits a small unusual positive curvature near T_c. In contrast to the curvature of B_{c2} and B_{c2}^*, which might indicate multiband superconductivity,[12] this curvature is caused by the double transition.

VII. CONCLUSIONS

In conclusion, we have carried out specific-heat and ac-susceptibility measurements on $PrOs_4Sb_{12}$. The deduced phase diagram confirms most of the published data. In both measurements a double transition could be observed and the two phase lines could be tracked down to $T=0.1$ K. The susceptibility measurement reveals enhanced pinning properties close to and below the lower of the two upper critical fields.

The specific-heat measurements exhibit an unusually rapid decrease of C below the superconducting transition, possibly pointing to pronounced strong-coupling superconductivity. An analysis with the α-model results in an extremely large gap ratio of $\Delta(0)/k_BT_c=3.7$ and a huge specific heat jump of $\Delta C/(\gamma T_c)\geqslant 5)$. The peaked shape of the specific-heat anomaly seems to reflect the rapid rise of condensed quasiparticles below T_c. The data demonstrate a moderately enhanced effective mass with a Sommerfeld coefficient of $0.15\ \mathrm{J\,K^{-2}\,mol^{-1}}<\gamma<0.35\ \mathrm{J\,K^{-2}\,mol^{-1}}$. The condensation energy at zero temperature amounts to roughly $200\ \mathrm{mJ/mol}<E_c<300\ \mathrm{mJ/mol}$ with a thermodynamic critical field of $B_c=0.04\pm0.02$ T.

ACKNOWLEDGMENTS

We thank P. Pfundstein and V. Ziebat for the microprobe analysis, and P. Adelmann and P. Schweiss for the x-ray diffraction studies. We acknowledge fruitful discussions with C. Meingast and P. Popovich. The work was supported by the Helmholtz Association of Research Centers VH-FZ-021. Research at UCSD was sponsored by the U.S. Department of Energy (DOE) under Research Grant No. DE-FG02-04ER46105 and the National Science Foundation (NSF) under Research Grant No. DMR 0335173.

*Present Address: Physics Departement E21, Technische Universität München, Germany

†Present Address: Los Alamos National Laboratory, Los Alamos, NM 87545, USA

[1] M. B. Maple, P.-C. Ho, V. S. Zapf, N. A. Frederick, E. D. Bauer, W. M. Yuhasz, F. M. Woodward, and J. W. Lynn, J. Phys. Soc. Jpn. **71**, Suppl., 23 (2002); Proceedings of the International Conference on Strongly Correlated Electrons with Orbital Degrees of Freedom (ORBITAL 2001).

[2] R. M. White and P. Fulde, Phys. Rev. Lett. **47**, 1540 (1981).

[3] R. Vollmer, A. Faißt, C. Pfleiderer, H. v. Löhneysen, E. D. Bauer, P.-C. Ho, V. Zapf, and M. B. Maple, Phys. Rev. Lett. **90**, 057001 (2003).

[4] T. Cichorek, A. C. Mota, F. Steglich, N. A. Frederick, W. M. Yuhasz, and M. B. Maple, Phys. Rev. Lett. **94**, 107002 (2005).

[5] E. E. M. Chia, M. B. Salamon, H. Sugawara, and H. Sato, Phys. Rev. Lett. **91**, 247003 (2003).

[6] K. Izawa, Y. Nakajima, J. Goryo, Y. Matsuda, S. Osaki, H. Sugawara, H. Sato, P. Thalmeier, and K. Maki, Phys. Rev. Lett. **90**, 117001 (2003).

[7] Y. Aoki, A. Tsuchiya, T. Kanayama, S. R. Saha, H. Sugawara, H. Sato, W. Higemoto, A. Koda, K. Ohishi, K. Nishiyama *et al.*, Phys. Rev. Lett. **91**, 067003 (2003).

[8] L. Shu, D. E. MacLaughlin, H. Heffner, G. D. Morris, O. O. Bernal, F. Callaghan, J. E. Sonier, A. Bosse, J. E. Anderson, W. M. Yuhasz, N. A. Frederick, and M. B. Maple, cond-mat/0502226 (2005).

[9] H. Kotegawa, M. Yogi, Y. Imamura, Y. Kawasaki, G.-q. Zheng, Y. Kitaoka, S. Ohsaki, H. Sugawara, Y. Aoki, and H. Sato, Phys. Rev. Lett. **90**, 027001 (2003).

[10] M. B. Maple, P.-C. Ho, N. A. Frederick, W. Y. V. S. Zapf, E. D. Bauer, A. D. Christianson, and A. H. Lacerda, J. Phys.: Condens. Matter **15**, S2071 (2003).

[11] N. A. Frederick, T. A. Sayles, and M. B. Maple, Phys. Rev. B **71**, 064508 (2005).

[12] M.-A. Measson, D. Braithwaite, J. Flouquet, G. Seyfarth, J. P. Brison, E. Lhotel, C. Paulsen, H. Sugawara, and H. Sato, Phys. Rev. B **70**, 064516 (2004).

[13] G. Seyfarth, J. Brison, M.-A. Measson, J. Flouquet, K. Izawa, Y. Matsuda, H. Sugawara, and H. Sato, cond-mat/0506522 v1 (2005).

[14] D. M. Broun, P. J. Turner, G. K. Mullins, D. E. Sheehy, X. G. Zheng, S. K. Kim, N. A. Frederick, M. B. Maple, W. N. Hardy, and D. A. Bonn, cond-mat/0310613 (2003).

[15] Y. Aoki, T. Namiki, H. S. S. Ohsaki, S. R. Saha, and H. Sato, J. Phys. Soc. Jpn. **71**, 2098 (2002).

[16] C. R. Rotundu, P. Kumar, and B. Andraka, cond-mat/0402599 (2004).

[17] N. Oeschler, P. Gegenwart, F. Weickert, I. Zerec, P. Thalmeier, F. Steglich, E. D. Bauer, N. A. Frederick, and M. B. Maple, Phys. Rev. B **69**, 235108 (2004).

[18] N. A. Frederick, T. D. Do, P.-C. Ho, N. P. Butch, V. S. Zapf, and M. B. Maple, Phys. Rev. B **69**, 024523 (2004).

[19] T. Tayama, T. Sakakibara, H. Sugawara, Y. Aoki, and H. Sato, J. Phys. Soc. Jpn. **72**, 1516 (2003).

[20] E. E. M. Chia, M. B. Salamon, H. Sugawara, and H. Sato, Phys. Rev. B **69**, 180509(R) (2004).

[21] H. Suderow, S. Vieira, J. D. Strand, S. Bud'ko, and P. C. Canfield,

Phys. Rev. B **69**, 060504(R) (2004).
[22] D. E. MacLaughlin, J. E. Sonier, R. H. Heffner, O. O. Bernal, B.-L. Young, M. S. Rose, G. D. Morris, E. D. Bauer, T. D. Do, and M. B. Maple, Phys. Rev. Lett. **89**, 157001 (2002).
[23] E. D. Bauer, N. A. Frederick, P.-C. Ho, V. S. Zapf, and M. B. Maple, Phys. Rev. B **65**, 100506(R) (2002).
[24] T. Goto, Y. Nemoto, K. Sakai, T. Yamaguchi, M. Akatsu, T. Yanagisawa, H. Hazama, K. Onuki, H. Sugawara, and H. Sato, Phys. Rev. B **69**, 180511(R) (2004).
[25] E. D. Bauer, A. Ślebarski, E. J. Freeman, C. Sirvent, and M. B. Maple, J. Phys.: Condens. Matter **13**, 4495 (2001), and references therein.
[26] P.-C. Ho, V. S. Zapf, E. D. Bauer, N. A. Frederick, M. B. Maple, G. Giester, P. Rogl, S. T. Berger, C. H. Paul, and E. Bauer, Int. J. Mod. Phys. B **16**, 3008 (2002).
[27] M. Kohgi, K. Iwasa, M. Nakajima, N. Metoki, S. Araki, N. Bernhoeft, J.-M. Mignot, A. Gukasov, H. Sato, Y. Aoki *et al.*, J. Phys. Soc. Jpn. **72**, 1002 (2003).
[28] E. A. Goremychkin, R. Osborn, E. D. Bauer, M. B. Maple, N. A. Frederick, W. M. Yuhasz, F. M. Woodward, and J. W. Lynn, Phys. Rev. Lett. **93**, 157003 (2004).
[29] K. Kuwahara, K. Iwasa, M. Kohgi, K. Kaneko, S. Araki, N. Metoki, H. Sugawara, Y. Aoki, and H. Sato, J. Phys. Soc. Jpn. **73**, 1439 (2004).
[30] H. Padamsee, J. E. Neighbor, and C. A. Shiffman, J. Low Temp. Phys. **12**, 387 (1973).
[31] B. Mühlschlegel, Z. Phys. **155**, 313 (1959).
[32] M. Tinkham, *Introduction To Superconductivity* (Dover, New York, 1996).
[33] C. Petrovic, P. G. Pagliuso, M. F. Hundley, R. Movshovich, J. L. Sarrao, J. D. Thompson, Z. Fisk, and P. Monthoux, J. Phys.: Condens. Matter **13**, L337 (2001).
[34] M. Yashima, M. Yashima, S. Kawasaki, Y. Kawasaki, G.-q. Zheng, Y. Kitaoka, H. Shishido, R. Settai, Y. Haga, and Y. Ōnuki, J. Phys. Soc. Jpn. **73**, 2073 (2004).
[35] F. Bouquet, Y. Wang, R. A. Fisher, D. G. Hinks, J. D. Jorgensen, A. Junod, and N. E. Phillips, Europhys. Lett. **56**, 856 (2001).
[36] K. Maki, H. Won, P. Thalmeier, Q. Yuan, K. Izawa, and Y. Matsuda, Europhys. Lett. **64**, 496 (2003).
[37] D. Parker, K. Maki, and S. Haas, cond-mat/0407254 v1 (2004).
[38] Y. Aoki, T. Namiki, S. Ohsaki, S. R. Saha, H. Sugawara, and H. Sato, Physica C **388-389**, 557 (2003).
[39] G. E. Volovik, JETP Lett. **58**, 469 (1993).
[40] M. Ichioka, A. Hasegawa, and K. Machida, Phys. Rev. B **59**, 184 (1999).
[41] F. Bouquet, Y. Wang, I. Sheikin, P. Toulemonde, M. Eisterer, H. Weber, S. Lee, S. Tajima, and A. Junod, Physica C **385**, 192 (2003).
[42] S. Drobnik, K. Grube, C. Pfleiderer, H. v. Löhneysen, E. D. Bauer, and M. Maple, Physica B **359-361**, 901 (2005).
[43] *Magnetic Susceptibility of Superconductors and Other Spin Systems*, edited by R. A. Hein, T. L. Francavilla, and D. H. Liebenberg (Plenum, New York, 1991).
[44] R. A. Hein and J. R. L. Falge, Phys. Rev. **123**, 407 (1961).
[45] Y. Haga, E. Yamamoto, Y. Inada, D. Aoki, K. Tenya, M. Ikeda, T. Sakakibara, and Y. Ōnuki1, J. Phys. Soc. Jpn. **65**, 3646 (1996).
[46] P.-C. Ho, N. A. Frederick, V. S. Zapf, E. D. Bauer, T. D. Do, M. B. Maple, A. D. Christianson, and A. H. Lacerda, Phys. Rev. B **67**, 180508(R) (2003).
[47] R. Radebaugh and P. H. Keesom, Phys. Rev. **149**, 217 (1966).
[48] M. A. Measson, J. P. Brison, G. Seyfarth, D. Braithwaite, G. Lapertot, B. Salce, J. Flouquet, E. Lhotel, C. Paulsen, H. Sugawara, H. Sato, P. C. Canfield, K. Izawa, and Y. Matsuda Physica B **359-361**, 827 (2005).
[49] N. Oeschler, P. Gegenwart, F. Steglich, N. A. Frederick, E. D. Bauer, and M. B. Maple, Acta Phys. Pol. B **34**, 959 (2003).
[50] H. Ullmaier, *Irreversible Properties of Type II Superconuctors* (Springer-Verlag, Berlin, 1975).
[51] R. R. Hake, Phys. Rev. **158**, 356 (1967).
[52] K. Maki, Phys. Rev. **148**, 362 (1966).